Journal of Magnetism and Magnetic Materials 474 (2019) 462–466

Contents lists available at ScienceDirect

Journal of Magnetism and Magnetic Materials

journal homepage: www.elsevier.com/locate/jmmm

Research articles

Field effect in the viscosity of magnetic colloids studied by multi-particle collision dynamics

Dmitry Zablotsky

University of Latvia, Raina bulv. 19, Riga LV-1586, Latvia

ARTICLE INFO

Keywords:
Ferrofluids
Magnetic colloids
Viscosity
Self-assembly

ABSTRACT

Colloidal solutions of magnetic nanoparticles are usually employed when the fluidity and magnetic properties are required at the same time, either in technical or biomedical applications. However, when the magnetic size of the nanoparticles is large enough (> 12–15 nm) the colloid may form an equilibrium structure with or without the external magnetic field, which can significantly influence its rheology. Using multi-particle collision dynamics we study the internal structure and viscosity of the magnetic colloids at varying magnitudes of the externally applied field. We show a generalized structural behavior across all studied regimes and an appreciable increase of flow resistance with magnetic field.

1. Introduction

Self-assembly is a major route by which colloids are able to organize into larger scale structures. The dipolar nanoparticles with sufficiently large dipole moments spontaneously form a polydisperse ensemble of stochastic flexible chains [1], which can be aligned and extended by external field. The possibility of these equilibrium formations was predicted theoretically [2] and evidenced by TEM in vitrified films [3–5] and SANS [6,7]. Magnetic colloids – solutions of magnetic nanoparticles – are unique in that they couple liquidity and magnetism. Field-induced structural anisotropy is apparent in the measurements of their rheological response [8,9] accompanied by a dramatic increase of viscosity and pronounced shear-thinning behavior as a consequence of the field-induced appearance and transformations of heterogeneous aggregates, where the presence of even minor amount of magnetic particles can have a profound influence on the flow behavior [10–13]. This self-assembled system represents strongly anisotropic reconfigurable material susceptible to external stimulation, which can be used to obtain negative-viscosity [14,15], create functional flow, perform immunoassay [16], administer drugs [17] or treat cancer [18]. The field-induced interactions are penetrating, reversible and can be switched on or off on demand without complicated chemistry. However, the safe and effective application of self-assembled materials in diverse fields relies on understanding and quantifying their macroscopic rheological behavior as a function of their internal microstructure. The flow behavior of strongly anisotropic materials with complex nonlinear rheology presents considerable problems, which cannot be solved without numerical simulations to resolve the interplay between long- and short-range anisotropic dipolar interactions, thermal fluctuations, solvent-mediated hydrodynamics and external field. Previously we have investigated the rheological response of dipolar colloids under infinite aligning field [13], however the effect of a finite field was not studied. Here we extend our simulation model and report the influence of a magnetic field with varying magnitude and direction on the structure and viscosity of ferrofluids.

2. Model

The dipolar colloids are modeled as an ensemble of monodisperse spheres with a diameter σ and an embedded point dipole $\boldsymbol{\mu}$ producing anisotropic pairwise interaction [19] ($\beta = (k_B T)^{-1}$) potential U_{dd}

$$\beta U_{dd}(\boldsymbol{\mu}_i, \boldsymbol{\mu}_j, \boldsymbol{r}_{ij}) = -\lambda \left[\frac{3(\boldsymbol{\mu}_i \cdot \boldsymbol{r}_{ij})(\boldsymbol{\mu}_j \cdot \boldsymbol{r}_{ij})}{r_{ij}^5} - \frac{\boldsymbol{\mu}_i \cdot \boldsymbol{\mu}_j}{r_{ij}^3} \right] \quad (1)$$

where $\boldsymbol{r}_{ij}$ is the center-to-center distance between particles i and j (all lengths are given in units of particle diameter σ). The dipole-dipole interaction parameter λ characterizes the ability of the colloid to form an equilibrium structure and expresses the ratio of the characteristic energy of the dipole-dipole interaction between the particles to the average energy of their thermal fluctuations:

$$\lambda = \frac{\mu_0}{4\pi} \frac{\beta \mu^2}{\sigma^3} \quad (2)$$

where μ_0 is the magnetic constant, μ – magnitude of the particle dipole moment, σ – the effective diameter of the particles, including the thickness of the surfactant shell. The excluded volume, incl. the steric

E-mail address: dmitrijs.zablockis@lu.lv.

https://doi.org/10.1016/j.jmmm.2018.10.065
Received 24 June 2018; Received in revised form 16 September 2018; Accepted 13 October 2018
Available online 19 October 2018
0304-8853/

hindrance of the solvation shell, is modeled by the repulsive Weeks-Chandler-Andersen (WCA) potential

$$\beta U_{WCA}(r_{ij}) = 4\left[(r_{ij})^{-12} - (r_{ij})^{-6} + \frac{1}{4}\right], \quad r_{ij} \leqslant \sqrt[6]{2} \tag{3}$$

To account for the hydrodynamic effects we use a hybrid scheme [20] whereby the interacting colloids are immersed in a coarse-grained fluid governed by the multi-particle collision dynamics (MPCD) [21,22], which employs a stochastic bath of point-particles with mass m_f to resolve the hydrodynamic modes on the desired length scale. In MPCD the dynamics proceeds in alternating streaming and collision steps. During the streaming the particles propagate ballistically during Δt_{mpcd}

$$\boldsymbol{r}_i(t + \Delta t_{mpcd}) = \boldsymbol{r}_i(t) + \Delta t_{mpcd}\boldsymbol{v}_i(t) \tag{4}$$

For the collision step the particles are assigned to cubic bins $a \times a \times a$ and their thermal velocities are transformed bin-wise to imitate multiparticle collisions

$$\boldsymbol{v}_i \to \langle \boldsymbol{v} \rangle_J + \kappa_J \boldsymbol{\Omega}_J(\alpha)\cdot(\boldsymbol{v}_i - \langle \boldsymbol{v} \rangle_J) \tag{5}$$

where $\boldsymbol{v}_i$ is the velocity of ith MPCD-particle in the Jth bin containing n_J particles, i.e. $i \in \{1,...,n_J\}$;$\langle \boldsymbol{v} \rangle_J = n_J^{-1}\sum_{i=1}^{n_J}\boldsymbol{v}_i$ is the average velocity and $\boldsymbol{\Omega}_J(\alpha)$ is the matrix for a rotation by an angle $\alpha = \frac{\pi}{2}$ around one of the six orthogonal axes aligned with the coordinate axes of the simulation box [21,23,20] randomly selected for every bin and collision step. The bin-wise scaling factor $\kappa_J = \sqrt{\frac{E}{E_J}}$, where $E_J = \frac{1}{2}\sum_{i=1}^{n_J} m_f \|\boldsymbol{v}_i - \langle \boldsymbol{v} \rangle_J\|^2$ – the kinetic energy of the particles in the bin and $E = \frac{3}{2}(n_J - 1)k_B T$, ensures a constant temperature T in NVT simulations. The local conservation of the streaming momentum leads to correct hydrodynamics on the length scales $r > a$. The colloid-solvent coupling is achieved at the streaming step [20] using the stochastic boundary conditions (BC) [24,20] to enforce the no-slip condition. Hence, the flow unbiased normal v_n and tangential v_τ velocities of the reflected solvent particles are drawn from the distributions

$$P(v_n) \propto v_n \exp\left(-\frac{1}{2}m_f\beta v_n^2\right), \quad P(v_\tau) \propto \exp\left(-\frac{1}{2}m_f\beta v_\tau^2\right) \tag{6}$$

Whereas the momentum exchanges impart force and torque on the colloids [20] enabling Brownian-like thermalization. The Mason number [25] (dimensionless shear rate) relates the destructive hydrodynamic forces to the bonding polarization forces

$$Mn = \frac{\pi\eta_0\sigma^3}{2\lambda k_B T}\dot{\gamma} \tag{7}$$

where η_0 is the viscosity of the solvent and $\dot{\gamma}$ is the shear rate. The simulations are performed with Large-scale Atomic/Molecular Massively Parallel Simulator (LAMMPS) [26,27], the dimensions of the simulation domain are $L_x = 24$, $L_y = 24$, $L_z = 24$ (volume $V = L_x L_y L_z$) containing 1320 colloids and approx. 630,000 solvent particles, the external field is applied in y direction, except when the direction is varied. In contrast to previous work [13], which exploits a rheometric channel geometry, here periodicity is imposed in all directions using Ewald's summation and metallic BCs to account for long-range dipolar interactions. Initially the colloids are randomly dispersed at a predefined volume fraction $\phi = 5$ vol%. The shear flow is induced using the Lees-Edwards scheme in y direction. As such, the current model is consistent with the bulk material flow and allows to study the effect of field strength and anisotropy. After a brief limit run the system was equilibrated for $t_{eq} = 4000\widetilde{t}$ followed by a production run of 4000–20, $000\widetilde{t}$, depending on the shear rate. Bin-wise sampling was used to measure the flow profile and determine the shear rate $\dot{\gamma}$. Every simulation was repeated between 4 and 32 times. The error is reported in terms of the standard deviation.

3. Results and discussion

Due to the presence of a moderate spontaneous dipole assigned to the nanoparticles, the system retains a limited structuring ability even in zero field, forming a small number of dynamic worm-like chains susceptible to intense thermal fluctuations. The action of the applied field $\xi = \mu_0\mu\beta H$ is twofold – to align the chains in the direction of the field and to suppress the rotational fluctuations of the constituent nanoparticles, whereas the latter effectively lowers the temperature of the system both stiffening the chains and elongating them along the field. Fig. 2B shows the probability distribution function (PDF) for finding particles belonging to chain-like structures at certain positions relative to the center of mass of the aggregates. With no external field the PDF is a compact isotropic spherical globule comprising shells of probability within which the orbital motion of the constituent nanoparticles proceeds during the rotational motion of the chains. The applied field effect on the averaged microstructure is visualized directly as initially the narrowing of the angular aperture available to the orientational fluctuations of the chains, whereas at high field the average conformations are essentially one-dimensional. The uncoiling and extension of the dissolved chain-like structures is accompanied by the appearance of additional orbits, which eventually transform into a set of narrow maximums within the elongating tail of the PDF where the particles are primarily localized in a chain.

The chain length distribution g_n expresses the number of n-particle chains within a unit volume of the colloid and is shown in Fig. 2 (left) for varying field strength. At all fields the chain length distribution is exponentially decaying with increasing number of constituent particles and comprises two regions with different slopes, the first dominated by the relatively short chains of a few particles and the second corresponding to a minor number of very long chains up to several tens of particles. As the field strength is increased $\xi \to \infty$ a larger quantity of longer chains is formed at the expense of free floating particles and shorter chains.

It was shown previously that the chain length distribution of dipolar colloids obtained at infinite field and varying dipolar strength λ and shear rates Mn shows a generalized behavior and obeys scaling relationships of the form $(\alpha_\lambda\alpha_{Mn}n, \beta_\lambda\alpha_{Mn}^{-1}\beta_{Mn}g_n)$, which can be used to obtain a master curve. Fig. 2 (middle) shows that the g_n dependence on the external field is collapsible as well across a broad range of shear rates $Mn \in \{10^{-5}, 1\}$ and field strengths $\xi \in \{0, \infty\}$ applying a scaling transformation $n^* = \alpha_\lambda\alpha_H\alpha_{Mn}n$ and $g_n^* = \beta_\lambda\beta_H\alpha_{Mn}^{-1}\beta_{Mn}g_n$, where α_λ, β_λ, α_{Mn}, β_{Mn} have been determined previously and α_H and β_H are used to reduce the field-dependence.

The average number of particles in a chain is expressed from the chain length distribution

$$\langle n \rangle = \frac{\sum_{n=1}^{\infty} n g_n}{\sum_{n=1}^{\infty} g_n} \tag{8}$$

The average length of a chain is just a few particles due to the overwhelming contribution of free-floating particles mixed with some amount of dimers, trimers etc. At low shear rate $Mn \to 0$ the self-assembled structure is relatively unaffected by the hydrodynamic stress exerted by the flow of the surrounding fluid and the average chain length does not change. For larger shear rates $Mn \to 1$ the shear forces become comparable with the magnetic forces keeping the chains together and the constituent particles can be more easily detached. The average chain length $\langle n \rangle$ decreases rapidly beyond approx. $Mn > 10^{-2}$. Fig. 2 (right) shows that at lower applied field magnitudes the chains are less susceptible to hydrodynamic erosion because their orientation is not completely fixed by the field and they retain a limited ability to align with the direction of the flow, which minimizes the hydrodynamic stress on the microstructure. When the rotation is impeded by the external field the erosion is more significant leading to a steep decrease of the chain length with the shear rate Mn. On average the chains are very

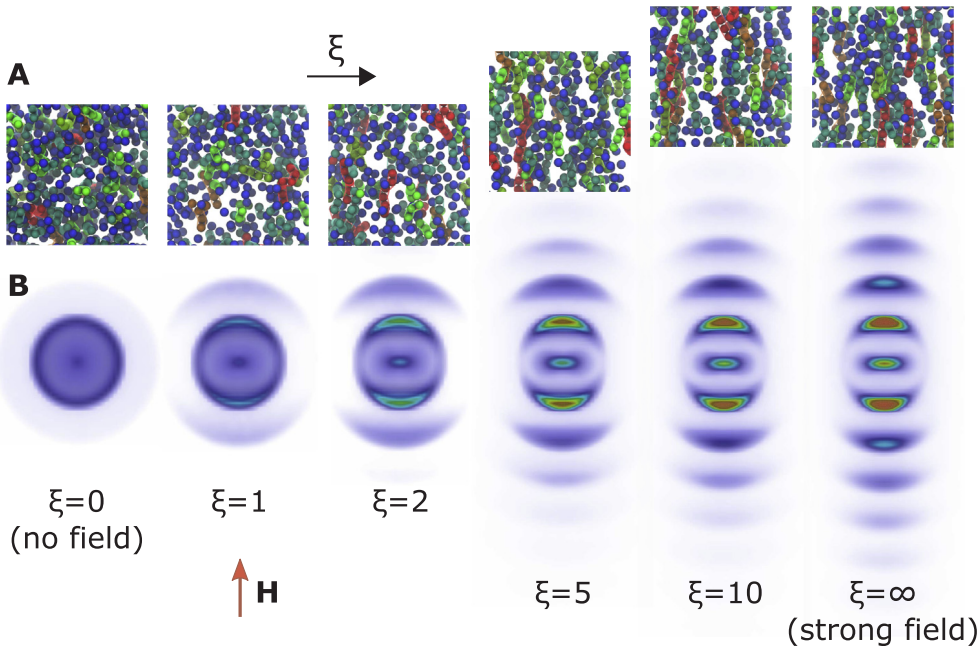

Fig. 1. Field-structured magnetic colloids ($\lambda = 3$): top (A) – simulation snapshots of self-assembled colloidal structures at increasing magnitude of magnetic field ξ; bottom (B) – corresponding positional probability distribution of particle within the self-assembled clusters.

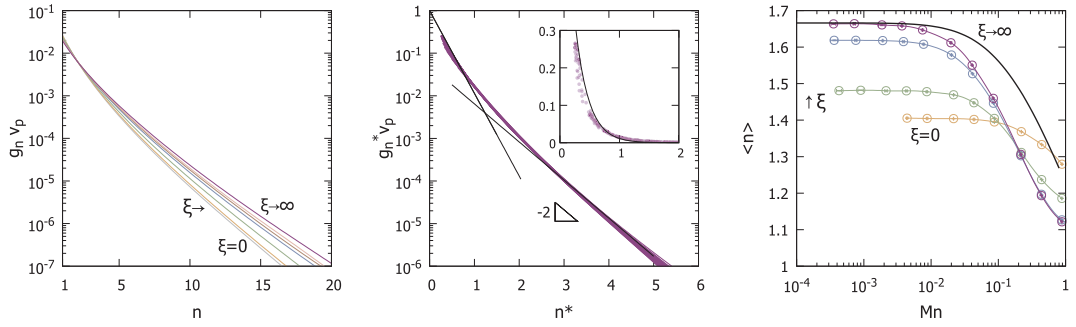

Fig. 2. Microstructure self-assembled from magnetic nanoparticles in shear flow and magnetic field ($\lambda = 3$): left – distribution of chain lengths g_n in vanishing shear $Mn \to 0$ and varying external field ξ; middle – chain length master curve obtained by plotting all simulation data for shear rates $Mn \in \{10^{-5}, 1\}$ and field strengths $\xi \in \{0, \infty\}$ in scaled coordinates (n^*, g_n^*), the inset shows a detailed view of the initial region; right – shear rate dependence of the average chain length $\langle n \rangle$ for varying field strength ξ.

short, of the order of $\langle n \rangle \propto 1 \div 2$ particles. This is, however, not representative of the magnitude of the magnetovisocus effect, which displays a variation of the intrinsic viscosity defined as (σ_{xy} is the shear stress)

$$[\eta] = \phi^{-1}\left(\frac{\sigma_{xy}}{\eta_0 \dot{\gamma}} - 1\right) \tag{9}$$

across more than an order of magnitude with the varying strength of the applied field in Fig. 3 (left). The contribution of the dissolved microstructure to the dissipation of streaming momentum characteristically scales as $[\eta] \propto n^3$ for the antisymmetric stress induced by the added torque of the orientationally fixed chains and $\propto \frac{n^3}{\log n}$ in the case of a symmetric stress increment, which is the conventional suspension stress [13]. Hence, the primary contributions to the viscosity come from the

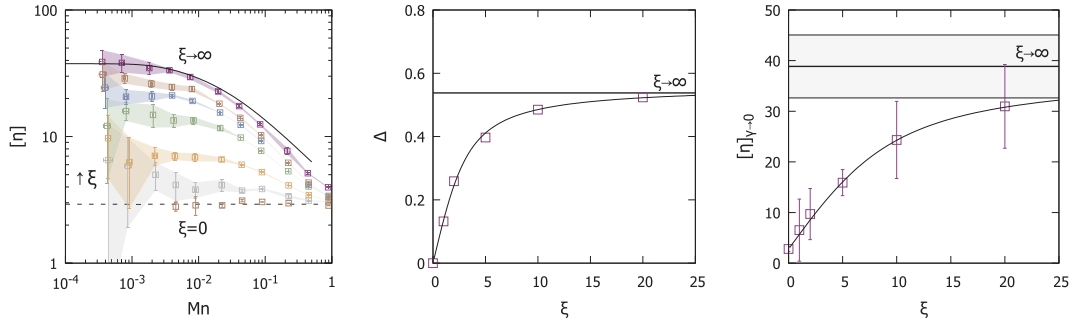

Fig. 3. Field dependence of the viscosity of ferrofluids ($\lambda = 3$): left – viscometric curves of the magnetic colloid obtained at varying field strength ξ; middle – dependence of the shear thinning exponent Δ on the applied field; right – field dependence of the viscosity at vanishing shear rate $Mn \to 0$.

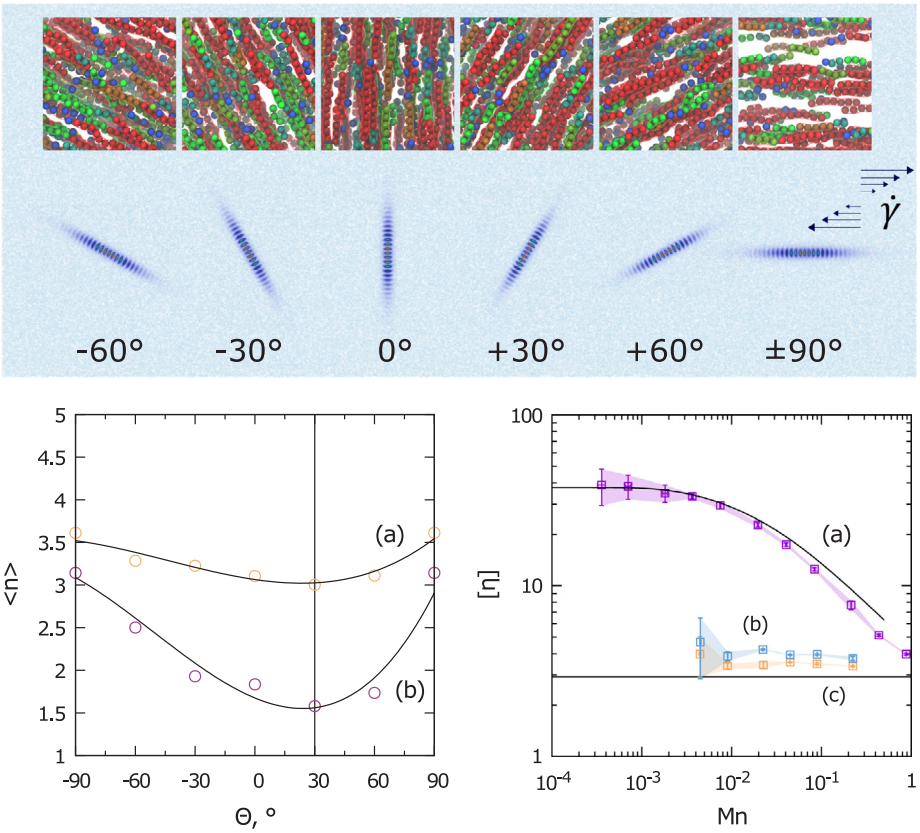

Fig. 4. Anisotropy of the chain – flow interactions ($\lambda = 4$): top – alignment of the dissolved microstructure relative to the shear flow by an inclined magnetic field and the corresponding probability density distribution, bottom: left – corresponding average chain length $\langle n \rangle$ (a) $Mn = 10^{-3}$, (b) $Mn = 0.1$; right – flow curves for magnetic field orientation along (a) velocity gradient, (b) velocity, (c) vorticity direction.

relatively rare events associated with the formation of very long chains $n \gg \langle n \rangle$.

At zero field the flow is nearly Newtonian although a limited degree of association can be seen from Figs. 1 and 2. With higher field strength a typical polymeric rheology is observed with a pseudo-Newtonian plateau at low shear rates leading to a near-power law $\propto Mn^{-\Delta}$ shear thinning region for $Mn \to 1$. The shear thinning exponent Δ here increases monotonously from 0 to a saturation value of about 0.538 (Fig. 3 (middle)), i.e. slightly less than approx. 0.8 found for dipolar colloids with high interaction strength $\lambda \to \infty$. For vanishing shear rates $Mn \to 0$, which is a typical regime for dispersions of nanosized particles, the intrinsic viscosity $[\eta]_{Mn \to 0}$ grows monotonically with the increasing field strength from approx. 3 at zero field ($\xi = 0$), which is slightly larger than 2.5 for non-magnetic suspensions, and slowly saturates at approx. 40 for $\xi \to \infty$ (Fig. 3 (right)) constituting more than one order of magnitude increase.

To check the anisotropy of the magnetic viscosity a series of simulated rheometric tests has been performed with varying orientation of a strong applied field relative to the direction of the shear. Fig. 4 indeed shows that the reference direction (0°), where the induction vector points along the velocity gradient, does indeed present by far the highest magnitude of the magnetoviscous effect, whereas other symmetric configurations – either along the direction of the velocity vector (90°) or the vorticity (perpendicular to both the velocity and the velocity gradient) vector – show negligible magnetic stress increment. Sweeping the magnetic field orientation from − 90° to 90° within the velocity-velocity gradient plane clearly reveals the asymmetry of the hydrodynamic stress. Mechanically, for inclination angles below 0° the hydrodynamic stress of the shear flow acting on a linear chain should be compressive, promoting the growth of chains, which are inclined opposite to the shearing direction. Likewise, for inclinations above 0° the stress should be erosive. Above approx. 30°, i.e. when the chains are slightly inclined in the direction of shear, the influence of the erosive stress reaches its maximum and starts to diminish with the reduction of the hydrodynamic cross-section of a chain, which is visible to the shear flow. Hence, the average chain length $\langle n \rangle$ begins to grow. The compressive effect is noticeable across a fairly broad range of studied shear rates ($Mn > 10^{-3}$).

4. Conclusions

Here we presented the initial results concerning the field dependence of viscosity of magnetic colloidal solutions (ferrofluids) with sufficient interaction strength to form a self-assembled microstructure. We have shown a generalized structural behavior where the chain-length distribution obeys a single master curve across all studied regimes of external field ξ and shear rate Mn. Subsequently, we have measured an appreciable increase of the flow resistance due to the extension of internal structure by magnetic field with an approximately twofold increase in the overall viscosity, which is characteristic for weakly-interacting commercial ferrofluids [8,28–30]. These results will serve as a basis for a more detailed theoretical analysis to produce a general framework for the rheology of field-structured colloids, which is currently underway. A potential difficulty is to account for the compressive influence of the shear flow on the self-assembled chain-like microstructure, which leads to artifacts in the existing tensorial models [31].

Acknowledgements

The support from the postdoctoral research program at the University of Latvia (project 1.1.1.2/VIAA/1/16/072) and M-ERA.NET

Project HarvEnPiez is gratefully acknowledged. The computing time of the LASC cluster was provided by the Institute of Solid State Physics (University of Latvia).

References

[1] K.I. Morozov, M.I. Shliomis, Ferrofluids: flexibility of magnetic particle chains, J. Phys.: Condens. Matter 16 (23) (2004) 3807–3818, https://doi.org/10.1088/0953-8984/16/23/001.

[2] P.G. Gennes, P.A. Pincus, Pair correlations in a ferromagnetic colloid, Physik der Kondensierten Materie 11 (3) (1970) 189–198, https://doi.org/10.1007/bf02422637.

[3] K. Butter, P. Bomans, P. Frederik, G. Vroege, A. Philipse, Direct observation of dipolar chains in iron ferrofluids by cryogenic electron microscopy, Nat. Mater. 2 (2) (2003) 88–91, https://doi.org/10.1038/nmat811.

[4] M. Klokkenburg, R.P.A. Dullens, W.K. Kegel, B.H. Erne, A.P. Philipse, Quantitative real-space analysis of self-assembled structures of magnetic dipolar colloids, Phys. Rev. Lett. 96 (3) (2006) 037203, https://doi.org/10.1103/physrevlett.96.037203.

[5] M. Klokkenburg, B.H. Erne, J.D. Meeldijk, A. Wiedenmann, A.V. Petukhov, R.P.A. Dullens, A.P. Philipse, In situ imaging of field-induced hexagonal columns in magnetite ferrofluids, Phys. Rev. Lett. 97 (18) (2006) 185702, https://doi.org/10.1103/physrevlett.97.185702.

[6] M. Klokkenburg, B.H. Erne, A. Wiedenmann, A.V. Petukhov, A.P. Philipse, Dipolar structures in magnetite ferrofluids studied with small-angle neutron scattering with and without applied magnetic field, Phys. Rev. E 75 (5) (2007) 051408, https://doi.org/10.1103/physreve.75.051408.

[7] M. Barrett, A. Deschner, J.P. Embs, M.C. Rheinstädter, Chain formation in a magnetic fluid under the influence of strong external magnetic fields studied by small angle neutron scattering, Soft Matter 7 (14) (2011) 6678, https://doi.org/10.1039/c1sm05104k.

[8] J. Linke, S. Odenbach, Anisotropy of the magnetoviscous effect in a ferrofluid with weakly interacting magnetite nanoparticles, J. Phys.: Condens. Matter 27 (17) (2015) 176001, https://doi.org/10.1088/0953-8984/27/17/176001.

[9] J. Linke, S. Odenbach, Anisotropy of the magnetoviscous effect in a cobalt ferrofluid with strong interparticle interaction, JMMM 396 (2015) 85–90, https://doi.org/10.1016/j.jmmm.2015.08.029.

[10] J. Nowak, D. Wolf, S. Odenbach, A rheological and microscopical characterization of biocompatible ferrofluids, JMMM 354 (2014) 98–104, https://doi.org/10.1016/j.jmmm.2013.10.050.

[11] M.T. Lopez-Lopez, A. Gomez-Ramirez, L. Rodriguez-Arco, J.D.G. Duran, L. Iskakova, A. Zubarev, Colloids on the frontier of ferrofluids. rheological properties, Langmuir 28 (15) (2012) 6232–6245, https://doi.org/10.1021/la204112w.

[12] D.I. Santiago-Quinonez, C. Rinaldi, Enhanced rheological properties of dilute suspensions of magnetic nanoparticles in a concentrated amphiphilic surfactant solution, Soft Matter 8 (19) (2012) 5327, https://doi.org/10.1039/c2sm07221a.

[13] D. Zablotsky, E. Blums, H.J. Herrmann, Self-assembly and rheology of dipolar colloids in simple shear studied using multi-particle collision dynamics, Soft Matter 13 (37) (2017) 6474–6489, https://doi.org/10.1039/c7sm00878c.

[14] J.-C. Bacri, R. Perzynski, M.I. Shliomis, G.I. Burde, “Negative-viscosity” effect in a magnetic fluid, Phys. Rev. Lett. 75 (11) (1995) 2128–2131, https://doi.org/10.1103/physrevlett.75.2128.

[15] J.E. Martin, K.J. Solis, Symmetry-breaking magnetic fields create a vortex fluid that exhibits a negative viscosity, active wetting, and strong mixing, Soft Matter 10 (22) (2014) 3993, https://doi.org/10.1039/c4sm00280f.

[16] F. Lacharme, C. Vandevyver, M.A.M. Gijs, Full on-chip nanoliter immunoassay by geometrical magnetic trapping of nanoparticle chains, Anal. Chem. 80 (8) (2008) 2905–2910, https://doi.org/10.1021/ac7020739.

[17] A.S. Lübbe, C. Alexiou, C. Bergemann, Clinical applications of magnetic drug targeting, J. Surg. Res. 95 (2) (2001) 200–206, https://doi.org/10.1006/jsre.2000.6030.

[18] I. Hilger, W. Andrä, R. Hergt, R. Hiergeist, H. Schubert, W.A. Kaiser, Electromagnetic heating of breast tumors in interventional radiology: in vitro and in vivo studies in human cadavers and mice, Radiology 218 (2) (2001) 570–575, https://doi.org/10.1148/radiology.218.2.r01fe19570.

[19] J.-J. Weis, D. Levesque, Simple dipolar fluids as generic models for soft matter, Adv. Polym. Sci. 185 (2005) 163–225, https://doi.org/10.1007/b136796.

[20] M. Hecht, J. Harting, T. Ihle, H.J. Herrmann, Simulation of claylike colloids, Phys. Rev. E 72 (1) (2005) 011408, https://doi.org/10.1103/physreve.72.011408.

[21] A. Malevanets, R. Kapral, Mesoscopic model for solvent dynamics, J. Chem. Phys. 110 (17) (1999) 8605–8613, https://doi.org/10.1063/1.478857.

[22] A. Malevanets, R. Kapral, Solute molecular dynamics in a mesoscale solvent, J. Chem. Phys. 112 (16) (2000) 7260–7269, https://doi.org/10.1063/1.481289.

[23] E. Tuzel, M. Strauss, T. Ihle, D.M. Kroll, Transport coefficients for stochastic rotation dynamics in three dimensions, Phys. Rev. E 68 (3) (2003) 036701, https://doi.org/10.1103/physreve.68.036701.

[24] Y. Inoue, Y. Chen, H. ohashi, Development of a simulation model for solid objects suspended in a fluctuating fluid, J. Stat. Phys. 107 (1) (2002) 85–100, https://doi.org/10.1023/A:1014550318814.

[25] C. Chaffey, S. Mason, Particle behavior in shear and electric fields, J. Colloid. Interface Sci. 27 (1) (1968) 115–126, https://doi.org/10.1016/0021-9797(68)90017-9.

[26] S. Plimpton, Fast parallel algorithms for short-range molecular dynamics, J. Comput. Phys. 117 (1) (1995) 1–19, https://doi.org/10.1006/jcph.1995.1039.

[27] M.K. Petersen, J.B. Lechman, S.J. Plimpton, G.S. Grest, P.J. in ’t Veld, P.R. Schunk, Mesoscale hydrodynamics via stochastic rotation dynamics: Comparison with lennard-jones fluid, J. Chem. Phys. 132 (2010) 174106.

[28] L. Pop, J. Hilljegerdes, S. Odenbach, A. Wiedenmann, The microstructure of ferrofluids and their rheological properties, Appl. Organometal. Chem. 18 (2004) 523–528, https://doi.org/10.1002/aoc.755.

[29] L.M. Pop, S. Odenbach, Investigation of the microscopic reason for the magnetoviscous effect in ferrofluids studied by small angle neutron scattering, J. Phys.: Condens. Matter 18 (2006) S2785, https://doi.org/10.1088/0953-8984/18/38/S17.

[30] L. Pop, S. Odenbach, Capillary viscosimetry on ferrofluids, J. Phys.: Condens. Matter 20 (2008) 204139, https://doi.org/10.1088/0953-8984/20/20/204139.

[31] H. See, Constitutive equation for electrorheological fluids based on the chain model, J. Phys. D: Appl. Phys. 33 (13) (2000) 1625–1633, https://doi.org/10.1088/0022-3727/33/13/311.